Hindawi
Mathematical Problems in Engineering
Volume 2018, Article ID 1652312, 16 pages
https://doi.org/10.1155/2018/1652312

Research Article

Effect of Shaft Pillar Extraction on Stability of Main Shaft: A Case Study at Xincheng Gold Mine, China

Xige Liu, Wancheng Zhu, Kai Guan, and Hongxun Zhang

Key Laboratory of Ministry of Education on Safe Mining of Deep Metal Mines, Northeastern University, Shenyang 110819, China

Correspondence should be addressed to Wancheng Zhu; zhuwancheng@mail.neu.edu.cn

Received 6 November 2017; Accepted 20 February 2018; Published 5 April 2018

Academic Editor: Xander Wang

Mining of ore body in the vicinity of a shaft has a significant influence on its stability. The in situ monitoring and numerical simulation are employed to analyze the effect of shaft pillar extraction at Xincheng Gold Mine. The XI# ore body is recently found around and beneath the shaft, and mining in this area may be detrimental to the shaft. Firstly, on the base of geological survey and in situ displacement monitoring, mechanical parameters of rock mass are obtained and the displacement around the shaft is measured. Secondly, the sensitivities of five main factors that may affect the shaft displacement are analyzed by means of orthogonal experiment according to the numerical simulation with FLAC^{3D}. Finally, a numerical model is established according to the in situ condition; in order to forecast the shaft displacement induced by mining activities of XI# orebody, the Mining Priority Index (MPI) is put forward and used to select the optimal mining sequence. Based on the comparison between the numerical results with the monitoring data, it is determined that the ore within 100 m from the shaft is not suggested to be extracted until the last period of the shaft life.

1. Introduction

Shafts are vital access ways for many underground mines, providing passageways for personnel, materials, and ventilation air. The shaft must be designed as a long-term workable and operational structure. As we know, a series of adverse factors threaten the stability of the shaft, such as faults, high geological stress, and mining activities. The conventional method of protecting vertical shafts and their associated service excavations from the mining disturbance is to leave a sufficient large pillar in the vicinity of the shaft. However, with the mining operation going deeper, sometimes fresh ore bodies may be found near the shaft; this is the case that happened at Xincheng Gold Mine, China. In this regard, the stability of shaft will be mainly concerned during the mining operations when the ore body near the shaft is going to be mined out. Furthermore, delineating a shaft pillar in conformity to a certain limit angle is the most common approach to be adopted for this issue. As a result, the amount of mineral resources cannot be mined out around the shaft, and the unworkable mineral will increase with the depth of the shaft. Therefore, this method is not applicable when the shaft depth is greater than 2.5 to 3.0 km in South Africa [1].

Recently, the downturn of the mining commodities price forces mining companies to extend the possible productivities, such as the ore body in the shaft pillar. As for the Xincheng Gold Mine in Shandong Gold Group, China, in recent years, the XI# ore body is found around the main production shaft that is currently used to hoist minerals from the V# ore body, Figure 1. In this regard, it is essential to keep the shaft workable and operational for a long time if the XI# ore body is intended to be mined out.

Many studies have been conducted on the mining operation of shaft pillars and a great number of experiences have been accumulated. Effects of the extraction of tabular deposits around vertical shafts in deep-level mines were numerically studied by Budavari and Croeser [1]; however, due to the limitation of the computing power and the difficulty in quantifying the rock mass parameters and specifying in situ stress conditions, the calculation results usually deviate from the in situ reality to some degree. When extracting the reef around the shaft at the start of mining operations, several

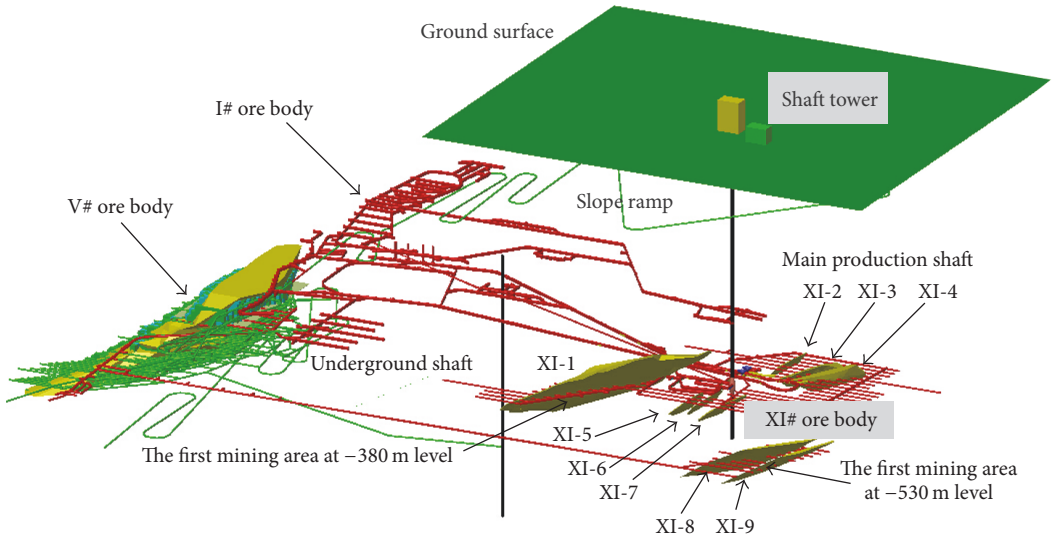

Figure 1: The overall layout of Xincheng Gold Mine.

alternatives to protect shaft pillars for deep vertical shaft systems were put forward [2], including the use of backfill, suitable mining layouts, and delaying shaft steelwork and lining installation until residual deformations are tolerable. A combination of strategically placed satellite pillars, yield pillars, and backfill method was chosen to protect the shaft from possible damaging stress changes and to minimize displacement in the shaft-reef area at Beatrix number 3 vertical shaft [3]. In Sumitomo Akabira Colliery, changing the displacement angle of the shaft pillar from 60° to 80°, the shaft damage was limited when the main fault crossing the shaft was considered as special attention [4]. Mining of the Ross pillar at Homestake Mine indicated that unexpected shaft wall movement could occur at a distance of 450 m from the current mining area [5]. A waste-cut across the shaft was proposed to extract the entire shaft pillar at the number 4 shaft of the African Rainbow Minerals (ARM) mine, which is located in highly stratified and poor-quality rock masses [6]. A shaft destressing slot is excavated to protect the main production shaft at Newmont Canada's Golden Giant Mine from potential damage from the high mining-induced stresses, and it allows the mine to extract a lot of high grade ore [7]. Degradation occurs to the X41 shaft at Copper Mine because of two major geological structures, the W41 and W42 faults, which intersect the shaft at two distinct locations [8, 9]. By virtue of the high geotechnic stress, serious deformation occurs during the sinking of a main shaft at Jinchuan Mine number 3; a tolerable deformation of 95 mm before lining is reasonable in order to maintain the shaft stability, as suggested by Zhao et al. [10]. In addition, it is noted that the dynamic interaction between the conveyances and the conveyance guiding system of aging mine shafts should be analyzed in order to examine the workability of shaft [11]. At Chengchao Iron Ore in China, the shaft exhibited evident degradation because of mining activities, Huang et al. [12] thought that the east shaft can continue to be used despite the surface subsidence rate of 0.314 mm/d and 0.144 mm/d in horizontal and vertical directions, respectively. Besides, some researches presented that lengthening or shortening the shaft lining by no more than 3 mm/m or 1 mm/m, respectively, generally does not cause sufficient damage to threaten the safety of shaft operations [13], and the shaft vertical displacement of 35 mm can be used as a threshold for lining damage of the X41 shaft at Copper Mine [8].

All of the case studies and above conclusions indicate that the extraction of shaft pillar is feasible if the sufficient measures such as backfilling, suitable mining layouts, and displacement monitoring are taken to mitigate the effect of mining operation on shaft displacement, even though in some cases shaft degradation occurs because of geological structures that are not clearly understood.

The theoretical analysis, in situ monitoring, and numerical methods are generally employed to examine the mining-induced responses to the shaft. Specifically, the theoretical model is of poor generality to represent the in situ condition of underground mining. The in situ monitoring could provide a lot of data, but they are sometimes difficult to be interpreted because dozens of uncertainties exist. On the other hand, the numerical simulation could give the prediction by using sophisticated numerical models; however, the rock mass parameters and in situ stress data are difficult to ensure accuracy and reliability. Therefore, the issue of shaft displacement and damage is complex, which should be solved by combining the performance of different methods. The solution strategy in this paper includes geological survey, in situ monitoring, and numerical simulation, hoping to achieve a better prediction of shaft deformation and to provide a reasonable suggestion to the mining operations.

2. Description of the Mine Site

The Xincheng Gold Mine is operated by Shandong Gold Group Co., Ltd, located in Shandong Province, China,

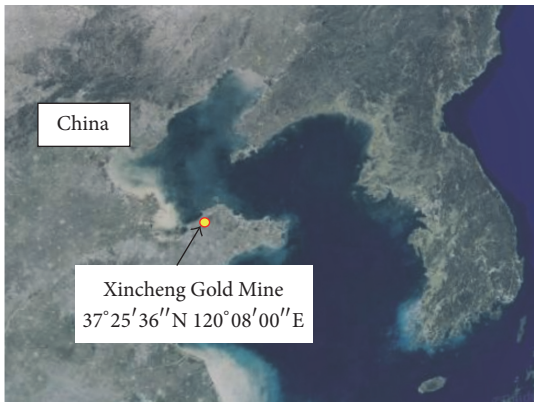

Figure 2: Location map of Xincheng Gold Mine in Shandong Province, China.

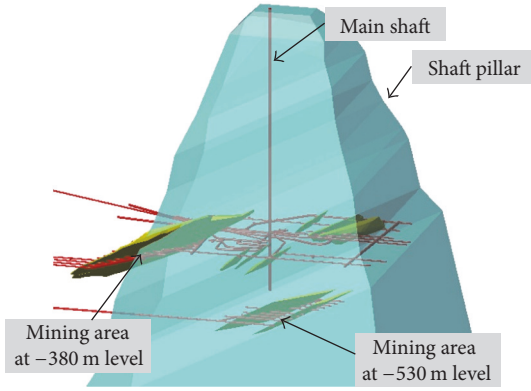

Figure 3: The XI# ore body and shaft pillar.

Figure 2. The construction of Xincheng Gold Mine started in 1975, and it was completed and put into production in 1980.

The shaft at Xincheng Gold Mine is 499 m deep, and the ground surface elevation is +33 m. According to the latest exploration near the main shaft, a new ore body numbered XI# that consists of 7 ore veins at −380 m level and 2 ore veins at −530 m level are found, Figure 1. Distribution of the XI# ore veins is scattered, the average strike is NE57°, and the dip of the veins is in the 25–30° range, which is parallel to the stratigraphic dip, and detailed information of the ore veins is listed in Table 1. In the beginning, a shaft pillar (Figure 3) has been delineated according to the respective rock movement angle of different strata, Table 2. Under these circumstances, more than 1140 kt ore cannot be mined out, which accounts for 67.4% of the XI# ore body. The first mining areas are designed in the XI-1 ore vein at −380 m level and in the XI-8 and XI-9 ore veins at −530 m level, and 280 kt ores have been mined out up to March, 2017. In order to protect the shaft, the following stopping sequence needs to be optimized and the stopping boundary needs to be determined.

The upward horizontal cut and backfill stopping method has been adopted for many years at Xincheng Gold Mine, and a wealth of experience has been accumulated. Compared with the open stopping method and stope caving method, the stopping-and-filling method is better in terms of maintaining the surrounding rock mass stable and preventing the surface subsidence. Therefore, this method is also adopted to excavate the XI# ore body in field production.

Table 1: Information of the XI# ore veins.

Vein number	Tonnage of ore/kt	Percentage/%	Distance from the shaft/m
XI-1	1174.51	69.43%	210
XI-2	7.84	0.46%	129
XI-3	49.87	2.95%	133
XI-4	75.55	4.47%	157
XI-5	40.28	2.38%	78
XI-6	4.96	0.29%	65
XI-7	49.87	2.95%	59
XI-8	155.90	9.22%	103
XI-9	132.92	7.86%	103
In total	1691.71	100.00%	-

3. Geological Survey

The detail rock mechanical parameters of the Xincheng Gold Mine were obtained during the shaft sinking which are listed in Table 2. The thickness of the quaternary surface soil is thin, while the bedrock is mainly magmatic rock and metamorphic rock with high mechanical strength, which are relatively intact, stable. Besides, the major geological structures in this area include the Jiaojia Fault, the Houjia Fault, and the Hexi Fault, as shown in the 155# vertical cross-section map, Figure 4. The Hexi Fault especially is close to the bottom of the shaft and overlapped with the ore veins XI-8 and XI-9 at −530 m level; thus, it needs to be given special attention. In fact, the three faults in this area are crushed zones with thickness of dozens of meters, rather than the general faults with the main fracture surfaces.

Former studies have shown that the horizontal geotechnic stress is significant at Xincheng Gold Mine [14], the σ_{max} and σ_{min} are both horizontal at the −280 m level and below, and the direction of σ_{max} is perpendicular to the strike of the strata, while the direction of σ_{min} is parallel to it contrastively. So, it can be further inferred that the faults in this area tend to be reverse faults, and this deduction provides a foundation for the follow-up analysis of the shaft stability. Thickness of the shaft liner is 0.3 m, and the net diameter is 5 m. Inside the shaft are a cage compartment, a ladder compartment, a skip compartment, and a pipe line compartment. Arrangement of the shaft section is depicted in Figure 5.

According to the Chinese relevant specification for protecting the mine shaft, when the rollers sliding along the steel shaft guides are used, the clearance of sliding guide groove on each side should be kept less than 10–15 mm in order to maintain the regular operation of the hoister in the shaft [15]. So the displacement of the main production shaft should not be larger than this threshold in order to guarantee the normal operation of the shaft. Currently, the hoister of the main production shaft runs well, indicating that the

Table 2: Main mechanical parameters of the rock samples retrieved around shaft.

Shaft depth/m	Lithology	Rock movement angle/°	Density/kg/m^3	Young's modulus/GPa	Poisson's ratio	UCS/MPa	Internal friction angle/°	Cohesion/MPa
0–33.80	Quaternary overburden	45	-	-	-	-	-	-
33.80–116.18	Cataclastic granite Sericitolite lithified granite Sericite & chlorite lithified granite	70	2490	42.7	0.18	50.3	35.75	40
116.18–168.00	Cataclastic granite	65	2570	96.8	0.36	46.4	36.5	32
168.00–225.00	Potassium feldspar & biotite lithified granite	80	2560	67.7	0.30	96.2	32.27	86
225.00–272.00	Sericitolite lithified mylonitic granite	70	2540	39.4	0.16	56.2	36.87	30
272.00–341.53	Sericitolite lithified mylonitic granite Pyritic phyllic cataclasite	65	2500	41.6	0.28	28.3	33.02	35
341.53–366.89	Pyritic phyllic granite Sericite & kaolin clay lithified granite	70	2530	46.4	0.16	41.6	33.02	38
366.89–422.00	Biotite granite Pyritic silicified granite	80	2580	48.2	0.16	79.4	36.87	48
422.00–465.50	Biotite granite	80	2620	49.4	0.18	78.9	33.82	59
465.50–529.74	Phyllic cataclastic granite Phyllic biotite granite	60	2630	78.8	0.24	63.5	33.22	41
529.74–663.20	Pyritic phyllic cataclasite Porphyritic granodiorite	80	2620	133.1	0.34	123.8	33.22	51

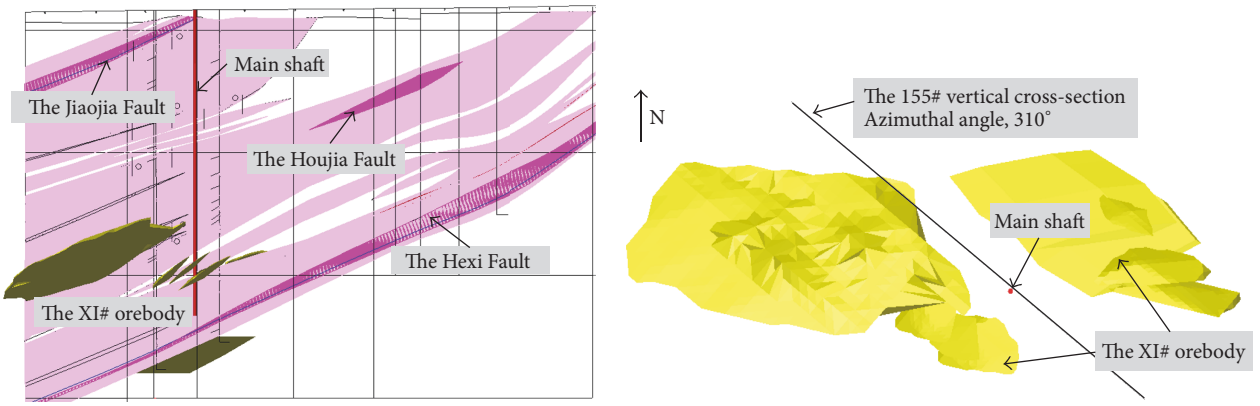

(a) Front view (b) Top view

Figure 4: The 155# vertical cross-section.

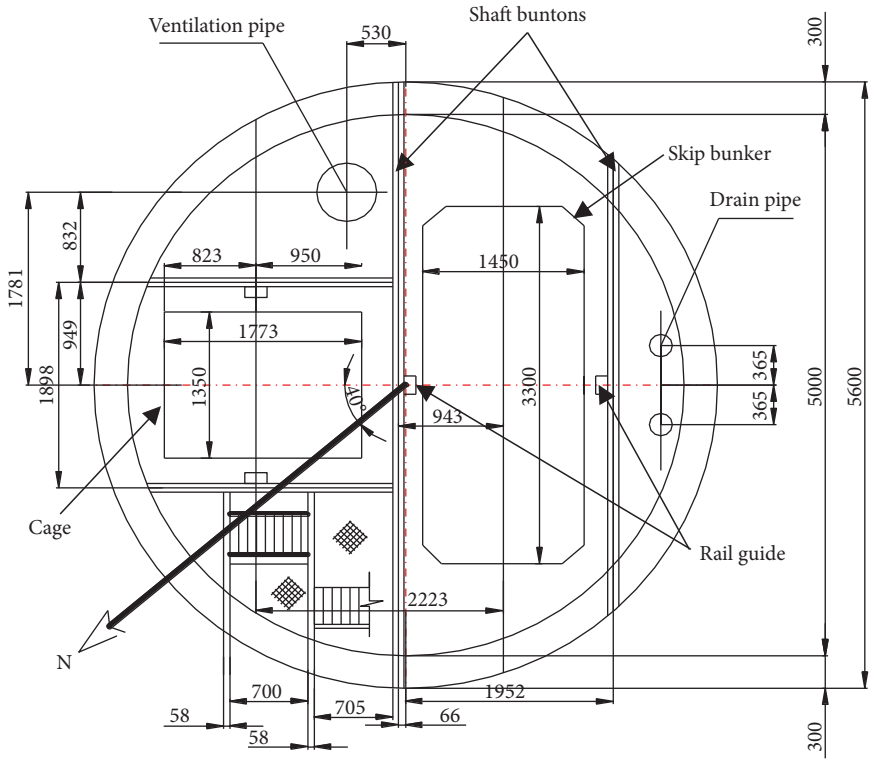

Figure 5: Cross-section diagram of the shaft.

clearance does not exceed the above-mentioned threshold. Most importantly, considering that the shaft will be used longer than 10 years, the 10 mm is selected as the upper limit for the shaft displacement, which is much less than the critical allowable displacement of the concrete liner.

4. In Situ Displacement Monitoring

In order to trace the response of the main production shaft at Xincheng Gold Mine during mining of the XI# ore body, it is essential to monitor the shaft displacement. In situ displacement monitoring can also provide data for validating the numerical simulation so as to improve the reliability of prediction. However, it is almost impossible to install monitoring equipment directly inside the shaft, because it may disturb the daily lifting operation. On the other hand, the shaft deformation is dependent on its adjacent rock stratum movement during underground excavation, and the method of monitoring the surrounding rock mass around the shaft is applied extensively to evaluate the displacement and stability of the shaft.

4.1. Installation of the Monitoring Equipment. The Sliding Micrometer, a high-precision strain meter (±0.002 mm/m),

Figure 6: On-site measurement using the Sliding Micrometer system.

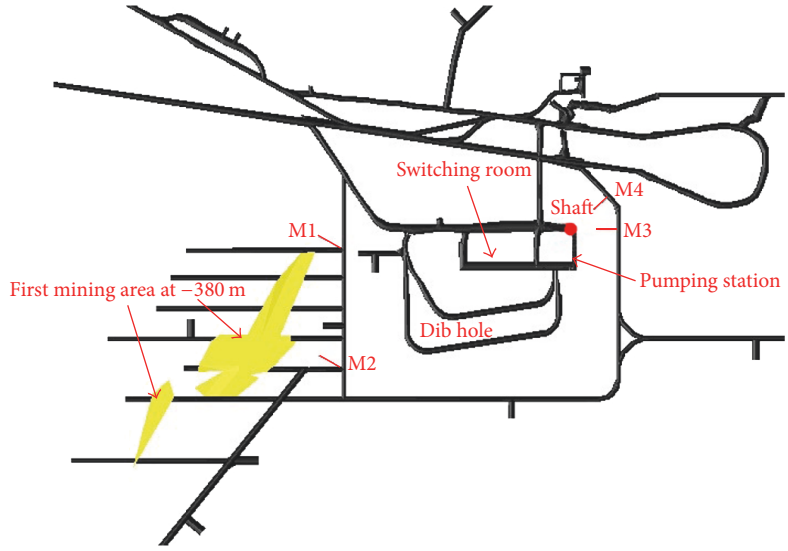

Figure 7: Arrangement of the 4 monitoring boreholes of Sliding Micrometer at −380 m level.

is applied to monitor the rock mass at −380 m level near the shaft. This monitoring system consists of the probe, cable, rod, readout unit, data-processing unit, and calibration device. It is noted that the probe uses the ball-and-cone positioning principle in the measuring marks of the measuring tube, and it needs regular calibration before and after each measurement.

4 Sliding Micrometer pipes, M1, M2, M3, and M4, were installed in the monitoring boreholes and then were grouted with cement mortar which should be cured for about 24 hours before measurement operate, in case the cement hardening may have detrimental influence on the monitoring displacement. On-site measurement diagram is shown in Figure 6. The 4 monitoring boreholes are horizontal and about 10–12 meters deep; boreholes M1 and M2 are near the XI# orebody and their borehole mouths are 110 m and 130 m far away from the shaft, respectively. Boreholes M3 and M4 are near the shaft and their bottoms are 7 m and 8 m from the shaft wall, Figure 7.

4.2. Monitoring Results. The initial monitoring values were collected on October 26, 2013, and the deformation of rock mass was obtained by subtracting the initial data from the subsequent monitored values. Excavating of the XI# ore body at −380 m level started on January 23, 2014. As of the latest collecting, March 27, 2017, more than 280 kt ores were mined out. The cumulative displacements of the 4 monitoring boreholes are shown in Figure 8. Positive value means tensile strain and the negative one stands for compressive strain.

Over more than the past three years, it is found that the max cumulative displacements at monitoring boreholes M1, M3, and M4 are 3.5 mm, −1.4 mm, and −0.3 mm, respectively, while M2 is up to 28.9 mm, because the borehole M2 was located in an isolated pillar after one slice of ore was mined out, Figure 7. However, as this mined-out area was backfilled, the displacement monitored at this borehole becomes stable, which indicates that the noticeable displacement monitored at M2 results from the mining activities. However, this mining-induced displacement in surrounding rock mass has little influence on the stability of shaft because the stope is far enough away from the protected shaft.

Correspondingly, the monitoring displacements of M3 and M4 (−1.4 mm and −0.3 mm) reflect the shaft displacement more directly; it indicates that the shaft displacement

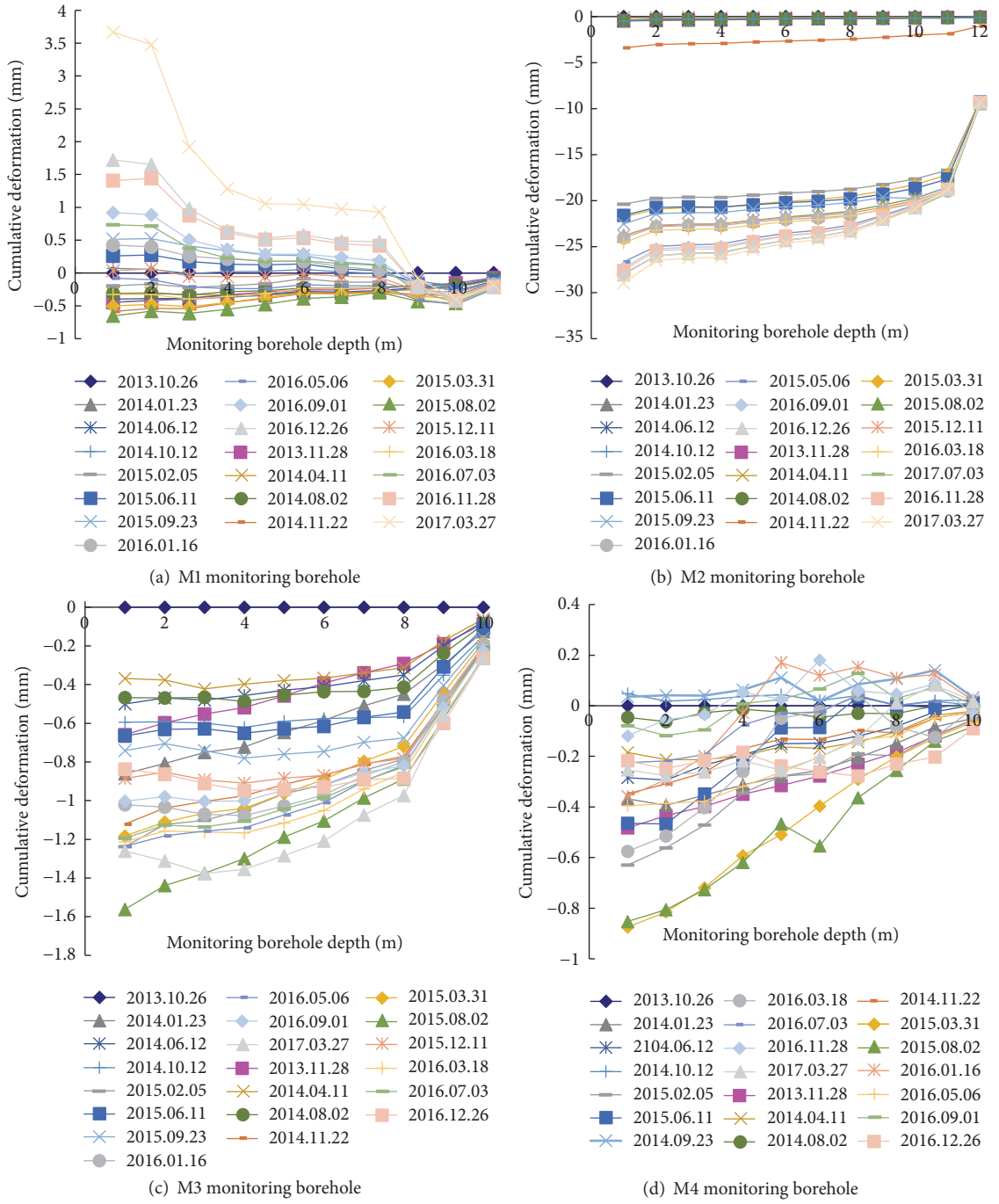

Figure 8: Cumulative displacement measured at 4 monitoring boreholes.

is much smaller than the threshold of 10 mm. Although a certain degree of fluctuation exists among the data during this monitoring period, according to the latest data, the max lateral displacement of shaft is 1.4 mm.

5. Sensitive Analysis of Factors Affecting the Shaft Displacement

The deformation mechanism of shaft can be very complicated; it is necessary to find the dominant factors affecting the shaft displacement based on a concept model. The influential factors include lithology of the rock mass, in situ stress state, mined-out area shape in terms of the ore body shape, location of the shaft, mining method and mining intensity, dynamic disturbances such as blasting vibration, special geological structure such as faults, groundwater, characteristics of the lining, service life, and maintenance. The concept of orthogonality is important in design of experiments because it says something about independence. Experimental analysis of an orthogonal design is usually straightforward because you can

Table 3: Mechanical parameters of the numerical orthogonal experimental.

Young's modulus/GPa	Poisson's ratio	Tensile strength/MPa	Internal friction angle/°	Cohesion/MPa	Density/kg/m^3
26	0.21	3.34	46.33	8.33	2650

Table 4: Design of factors and levels for the orthogonal experimental design.

Levels	Factors				
	Lateral pressure coefficient/λ	Dip/°	Thickness/m	Distance/m	Location
1	1.0	20	10	50	Hanging wall
2	1.5	45	20	100	Footwall
3	2.0	70	30	150	

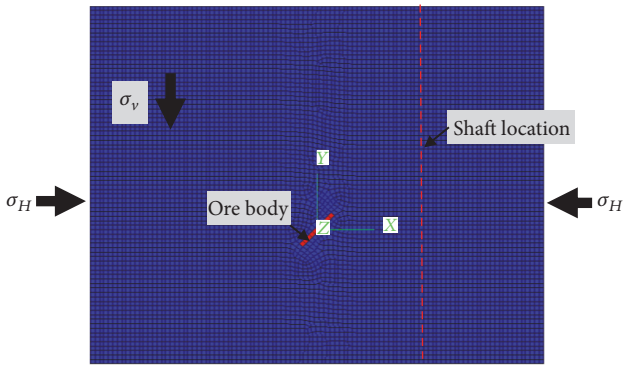

Figure 9: Numerical model of FLAC^{3D} of the concept model.

estimate each main effect and interaction independently. In this section, orthogonal experimental design was used to find the dominant one that affects the shaft displacement remarkably.

5.1. Orthogonal Experimental Design. The orthogonal numerical experiment has been done in virtue of the calculation of different scenarios with FLAC^{3D} software, as shown in Figure 9, and the numerical model is simplified to be a conceptual model in plain strain condition, whose size is 1000 m $*$ 800 m $*$ 20 m, and the 3rd dimension is just 20 m, in which direction the displacement is not concerned in this simplified model; in this respect, a 2D model may be also acceptable for this case. And the shaft is not considered in the grid of FLA3D in order to eliminate the error that may be induced because its diameter of 5 m is too small to be considered. In this respect, the displacement of the shaft is interpolated from the nodes nearby. The maximum and minimum principal stresses occur in the X and Y directions while the gravitational stress is applied along the Z direction, specifically, $\sigma_v = \gamma H$, $\sigma_H = \lambda\gamma H$ (λ = 1.0, 1.5, and 2.0, as shown in Table 4), and $\sigma_h = 0.5\gamma H$. The stress boundary conditions are adopted for the two numerical models in this paper, and when the calculation reached an equilibrium status, the initial displacements are set to zero, and then, the new displacements are considered to be caused by mining activities, because this numerical model is only a simplified concept model, primarily aimed at finding the dominant factors affecting the shaft displacement in general situations and providing useful references to the researchers. Referring to the rock mechanics parameters of Xincheng Gold Mine, the orebody and surrounding rock mass are of the similar lithology in this model, as listed in Table 3.

Selecting the lateral pressure coefficient of the in situ stress state, distance between the shaft and mined-out area, location of the shaft (at the footwall or hanging wall of ore body), dip of ore body, and thickness of ore body as controllable factors in the orthogonal experiments and the levels of these factors are designed and listed in Table 4.

5.2. Orthogonal Experimental Results. The orthogonal table L_{18} (2×3^7) is applied and the result is shown in Table 5. Through the analysis of Fisher's F distribution, numerical results indicate that dip of the ore body, lateral pressure coefficient, and distance between the shaft and mined-out area are significant factors affecting the shaft displacement. In contrast, thickness of the ore body and the location of the shaft are indistinctive. On condition that the shaft is located at the hanging wall, the deformation region is more extensive than that at the footwall, as shown in Figure 10.

Based on this orthogonal experiment, the dip of the ore body, lateral pressure coefficient, and distance between the shaft and mined-out area are specially considered in the later numerical simulation. In particular, the mining activity is most closely relevant to the distance between the mining stope and the shaft.

6. Numerical Analyze of the Shaft Stability

6.1. Modelling Strategy. A bigger numerical model of the Xincheng Gold Mine was established subsequently, whose size is 1000 m $*$ 1200 m $*$ 1000 m, Figure 11; X is the strike direction, Y is the dip direction, and Z is the gravity direction. The Hexi Fault is adjacent to the bottom of the shaft and overlaps with the XI-8 and XI-9 ore veins at −530 m level, so it is meshed intensively. As a matter of fact, the Hexi Fault is a crushed zone with thickness of dozens of meters, rather than a general fault with the main fracture surfaces. Thus, the "interface" element is not adopted in this model; instead, it is embodied through a series of weaker mechanical parameters; as shown in Table 6, the buried depth from 465.50 to 529.74

Table 5: Variance analysis of the orthogonal experiment.

Source of the variance	Quadratic sum	Degrees of freedom	Mean sum of square	F	F_α	Significance
Lateral pressure	0.002088	2	0.001044	12.626479	3.98	Very high
Distance	0.002317	2	0.001158	14.006953	3.98	Very high
Dip	0.003780	2	0.001890	22.855622	3.98	Very high
Thickness	0.000168	2	0.000084			Low
Location$^{\triangle}$	0.000047	1	0.000047			Low
$e^{\triangle}$	0.000694	8	0.000087			Low
e'	0.000910	11	0.000083			Low
In total	0.010005	17				Low

"△" indicate that the mean sum of square of this factor is smaller than that of error term, being incorporated into the error term.

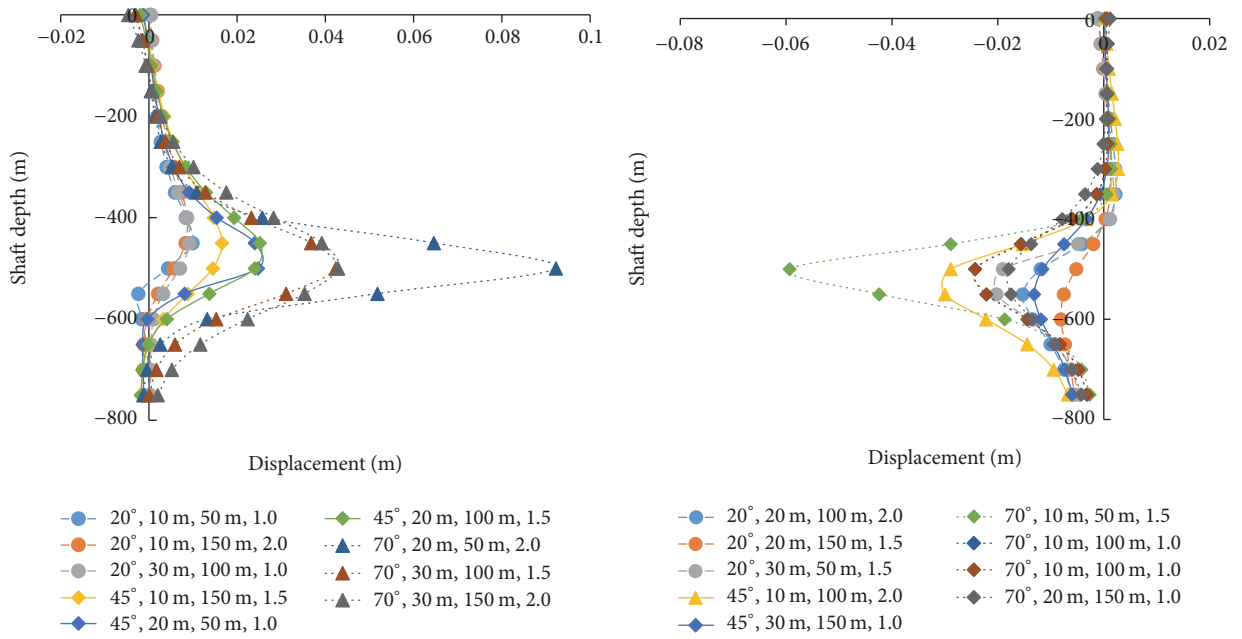

(a) The shaft at the hanging wall

(b) The shaft at the footwall

Figure 10: Shaft displacement for different depths, the legend "20°, 10 m, 50 m, 1.0" means the dip and thickness of orebody are 20° and 10 m, the distance between the ore and shaft is 50 m, and the lateral pressure coefficient is 1.0.

is the location of Hexi Fault. The same method is also applied to the other two faults.

The ideal elastic-plastic model with Mohr-Coulomb yield surface in the FLAC^{3D} software is adopted, that is,

$$f = \sigma_1 - \sigma_3 \frac{1 + \sin\varphi}{1 - \sin\varphi} - 2c\sqrt{\frac{1 + \sin\varphi}{1 - \sin\varphi}}, \quad (1)$$

where σ_1 and σ_3 are the maximum and minimum principal stress, respectively, c is internal cohesive force, and ϕ is angle of internal friction. When $f > 0$, failure occurs.

6.2. Mechanical Parameters of Rock Mass. The modified Hoek-Brown criterion with the RocLab software [16] is applied to obtain the reasonable rock mass parameters, which is expressed as

$$\sigma_1 = \sigma_3 + \sigma_c \left(m_b \frac{\sigma_3}{\sigma_c} + s \right)^{\alpha}, \quad (2)$$

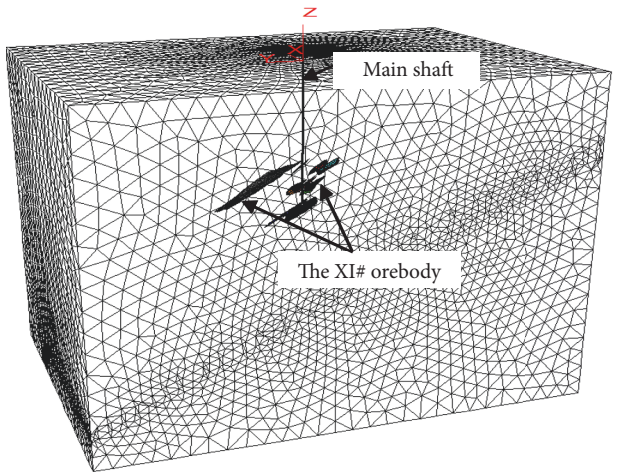

Figure 11: The overall numerical model of Xincheng Gold Mine.

Table 6: Mechanical parameters of rock mass calculated according to Hoek-Brown criterion.

Shaft depth/m	m_i	GSI	UCS/MPa	D	Young's modulus/GPa	Internal friction angle/°	Poisson's ratio	Cohesion/MPa	Tensile strength/MPa
0–33.80	-*	-	-	-	8.04	42	0.29	2.00	0.05
33.80–116.18	33	60	50.3	0	12.61	43.84	0.18	4.08	0.075
116.18–168.00	33	65	46.4	0	16.15	45.30	0.36	4.01	0.1
168.00–225.00	33	70	96.2	0	30.02	46.74	0.30	8.90	0.304
225.00–272.00	33	70	56.2	0	23.71	46.74	0.16	5.20	0.177
272.00–341.53	33	65	28.3	0	12.62	45.30	0.28	2.45	0.061
341.53–366.89	33	70	41.6	0	20.40	46.74	0.16	3.85	0.131
366.89–422.00	33	75	79.4	0	37.58	48.15	0.16	7.90	0.365
422.00–465.50	33	75	78.9	0	37.46	48.15	0.18	7.85	0.363
465.50–529.74	33	60	63.5	0	14.17	43.84	0.24	5.14	0.094
529.74–663.20	30	70	123.8	0	31.62	45.94	0.34	11.19	0.43

*Intact rock core cannot be obtained in the stratum from 0 to 33.8 m beneath the surface.

where m_b is a reduced value of the material constant m_i as given by

$$m_b = m_i \exp\left(\frac{\mathrm{GSI} - 100}{28 - 14D}\right), \tag{3}$$

and s and α are constants for the rock mass given by

$$s = \exp\left(\frac{\mathrm{GSI} - 100}{9 - 3D}\right),$$
$$\alpha = \frac{1}{2} + \frac{1}{6}\left[\exp\left(\frac{-\mathrm{GSI}}{15}\right) - \exp\left(\frac{-20}{3}\right)\right]; \tag{4}$$

D is a factor which depends upon the degree of disturbance, it varies from 0 for undisturbed in situ rock masses to 1 for much disturbed rock masses, m_i is a material constant according to the lithology, and geological strength index (GSI) was introduced to quantify the rock mass and surface conditions of the discontinuities.

In this study, rock masses are treated as undisturbed materials; namely, $D = 0$ is set for all of the rock strata around the shaft, σ_c is the uniaxial compressive strength (UCS) of the intact rock, and m_i can be selected according to Table 2. The values of geological strength index GSI cannot be obtained directly; they must be obtained based on in situ investigation of the rock mass around the shaft. However, it is scarcely possible to scan the joints and fissures on the surface of the shaft. Therefore, the in situ survey work was conducted in the drifts near the shaft.

The rock joints and interfaces at the drifts surface of all of the strata are scanned by using the ShapeMetriX3D system (Austrian Startup Company, 2008), and then, a 3D digital image of the surface containing the joints information can be built, as shown in Figure 12. Based on this real 3D rock surface, some visible rock mass features, such as the orientations, traces, areas, lengths, and position of joints, are retrieved. In addition, according to the field investigation, the GSI values of the rock mass around the shaft are estimated based on the geological descriptions in [17]. The mechanical parameters of all the rock strata are listed in Table 6.

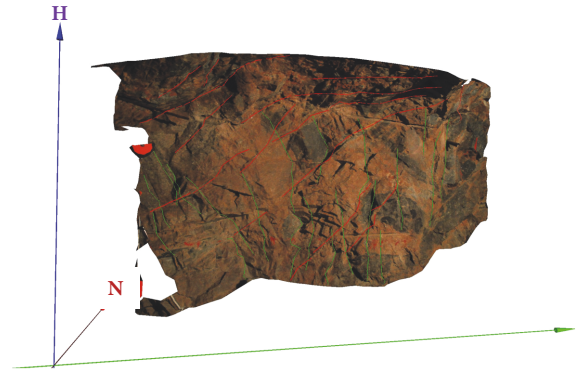

Figure 12: Joint sets (indicated in red and green colors) retrieved with ShapeMetriX3D.

Due to the difference of strata, the premining stress distribution depends on both depth and rock properties [18], as shown in Figure 13. Obviously, by using the stress boundary conditions, when the calculation reaches to an equilibrium status, the strata with higher Young's modulus hold higher stress than the rest of the geological formations.

6.3. Simulated Mining Sequence. Limited by the computing ability of computer, this big numerical model, Figure 11, is difficult to be established so meticulously. As a result, it aims to give advices on the mining sequence from a macroscopic view at present, and the simulative excavation scope of each step is large.

In the numerical simulation, scenario I is approaching to the shaft gradually, which is advantageous for stopping mining according to the shaft displacement, and it consists of 6 steps, Figure 14(a). Firstly, the XI-1, XI-2, XI-3, and XI-4 veins at −380 m level are mined in 4 steps towards the main shaft until a distance of 100 m; and then, the XI-8 and XI-9 veins at −530 m level are extracted; at last, the rest of the orebodies within 100 m distance from the shaft, including XI-5, XI-6, and XI-7 ore veins and a small part of the XI-1 vein,

Table 7: Details of scenario I.

Simulative excavating steps	Mineral output/kt	Ore proportion/%	Shaft displacement/m	displacement proportion/%	MPI
1	264.19	15.62%	0.001236	10.07%	1.55
2	363.85	21.51%	0.002031	16.55%	1.30
3	373.34	22.07%	0.003656	29.80%	0.74
4	295.83	17.49%	0.003887	31.68%	0.55
5	289.31	17.10%	−0.00022	−1.79%	−9.55
6	105.20	6.22%	0.00168	13.69%	0.45
In total	1691.71	100%	0.01227	100%	1.00

Table 8: Backfilling mechanical parameters in the numerical simulation.

Material	Density/kg/m^3	Young's modulus/GPa	Poisson's ratio	UCS/MPa	Internal friction angle/°	Cohesion/MPa
Backfilling	2020	1.21	0.28	2	40	0.5

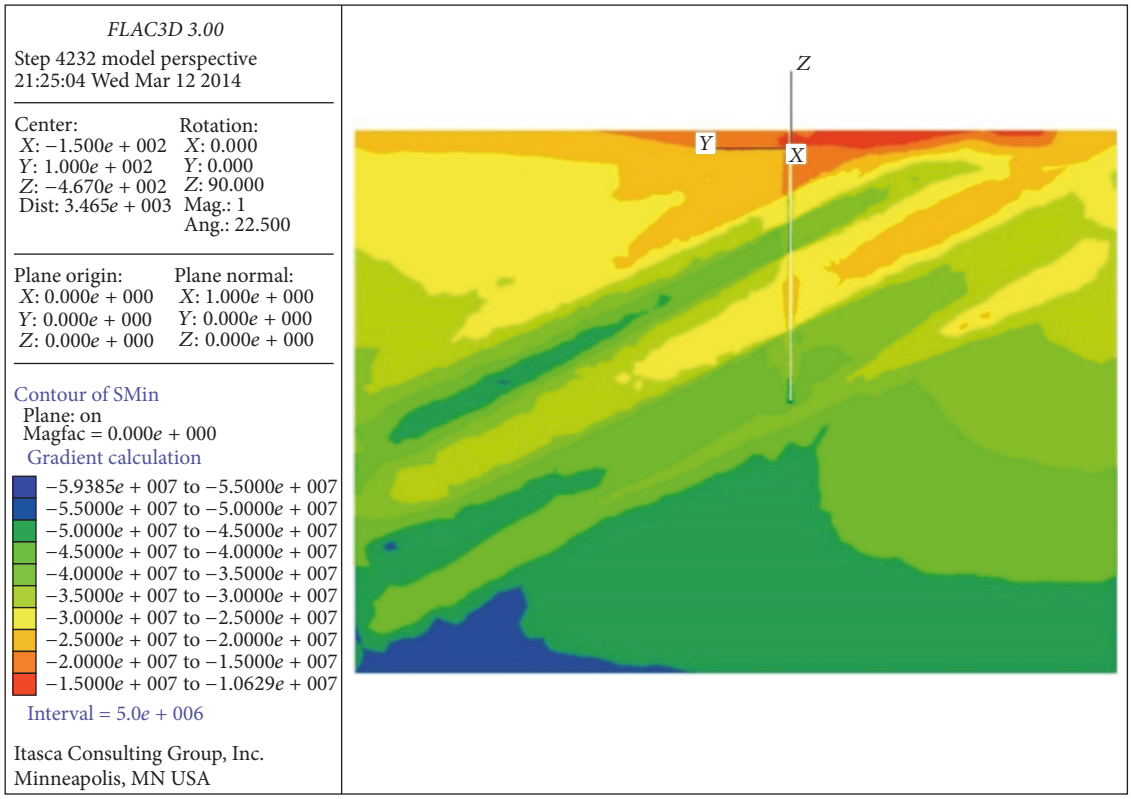

Figure 13: Contour of initial maximum principal stress.

are extracted. The output ore at each step is listed in Table 7. Besides, backfilling is simulated to be completed before the next step of extraction, whose mechanical parameters are listed in Table 8.

6.4. Numerical Simulation Results. When the ore is mined out completely, the contour of displacement field is illustrated in Figure 15. Rock mass tends to move towards the mined-out area, and the maximum displacement occurs in the hanging wall, reaching to 56.7 mm. Because the shaft locates at the footwall of the XI# ore body, the excavation leads to a limited influence on it. However, due to high horizontal in situ stress and the mining activities, the Hexi Fault distorts seriously; as a result, the displacement of the shaft bottom is up to 12 mm.

Figure 16 shows the displacement along the lateral (strike, dip) and vertical direction, respectively. It is shown that the lateral displacement accounts for a significant proportion in the total displacement of the shaft. Lateral distortion along the strike direction is no more than 3 mm even when the XI# ore body is excavated completely. In contrast, the lateral distortion along the dip direction is much more serious, which exceeds 10 mm at the shaft bottom. In the vertical

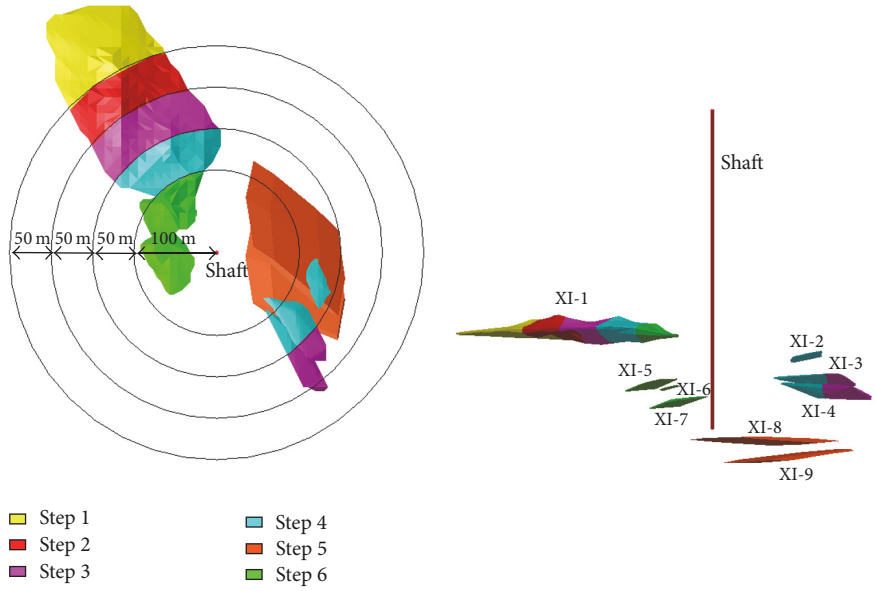

(a) Scenario I

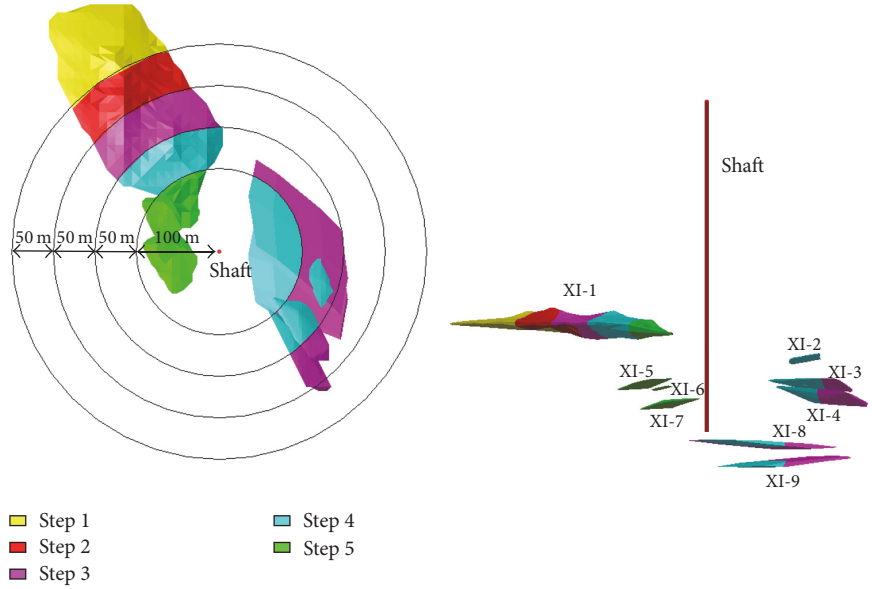

(b) Scenario II

Figure 14: Mining scenarios for the numerical simulation.

direction, subsidence occurs mainly at the upper part of the shaft and floor heaving occurs at the shaft bottom, which is consistent with the contour of displacement shown in Figure 15.

Besides, the displacements of the shaft are recorded during excavation at the foreshaft, −270 m level, −380 m level, and the bottom, respectively, Figure 17(a). It indicates that the shaft displacements at the foreshaft and −270 m level increase slowly until 3.5 mm, while the displacement at −380 m level and the shaft bottom increases rapidly. Particularly in the last few mining steps, the maximum displacement which occurs at the shaft bottom exceeds the safety threshold 10 mm when the whole orebody is mined out. It is worth mentioning that spring-back displacement occurs after excavating the XI-8 and XI-9 veins (Step 5), which indicates that the mining sequence outlined in scenario I is required to be optimized, in order to control the shaft displacement under the threshold of 10 mm.

Since both the ore production and the corresponding displacement of shaft are different in each mining step, it is difficult to draw a conclusion directly. In order to quantify the relationship between ore production and shaft displacement, a Mining Priority Index (MPI) which is described as the ratio between percentage of ore production and the percentage of

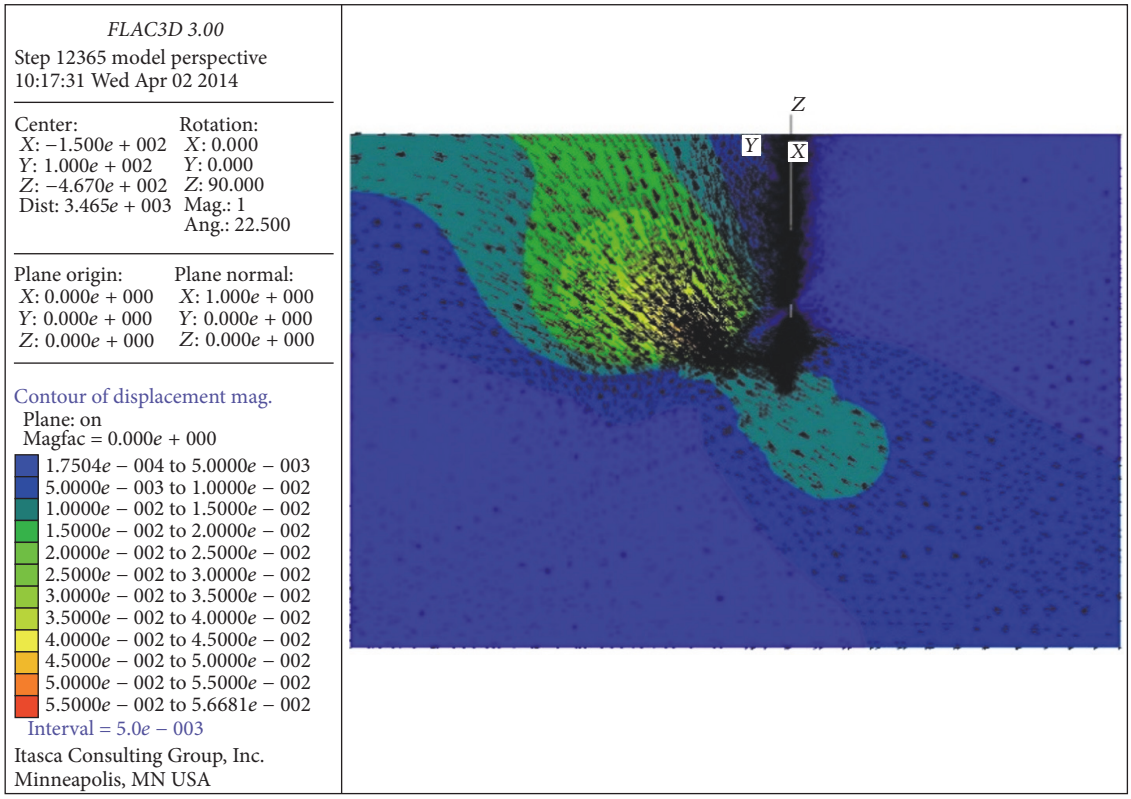

Figure 15: Contour of maximum displacement.

the induced maximum incremental displacement of shaft in each mining step, is defined.

$$\text{Mining Priority Index (MPI)} = \frac{\text{Ore production percentage}}{\text{Shaft deformation percentage}}. \quad (5)$$

Just as the definition implies, the higher the MPI is, the smaller the incremental shaft displacement occurs when the ore production remains the same, or more ores will be mined out if the incremental shaft displacement remains constant. Substantially, the MPI value is a comprehensive evaluation index considering both the economic benefit and the safety of shaft. Obviously, the overall MPI value of the XI# ore body is 1 (100% to 100%). If the MPI is larger than 1, excavating this part of ore body is relatively better than the others. Otherwise, the mining conditions may be worse, especially, if the MPI value is negative, indicating that this mining step is not reasonable; namely, spring-back shaft displacement occurs.

Table 7 shows information of the scenario I that the MPI values declines gradually with mining operation, indicating that the overall mining sequence, excavating approaching to the shaft, is reasonable. However, the negative MPI value which appeared at step 5 indicates that the excavating of XI-8 and XI-9 veins should be coordinated in order to avoid this kind of excavation.

The modified mining sequence scenario II is to extract the XI-8 and XI-9 veins (Step 5) together with step 3 and step 4, Figure 12(b), while other steps stay the same as the scenario I; thus, only 5 steps are left in the scenario II. As for the scenario II, the orebodies XI-1 and XI-2, XI-3, XI-4, XI-8, and XI-9 at two sides of the shaft are mined simultaneously, which may be better for balancing the possible tilt of shaft. The relevant displacement results are shown in Figures 17(b) and 18, and the maximum displacement (at the shaft bottom) does not exceed 10 mm if all the orebody is mined out for the scenario II.

For the scenario II, the deformation patterns along the shaft depth change a little but the maximum shaft displacement decreases evidently. The MPI values are listed in Table 9; negative values do not emerge; correspondingly, displacement of the shaft also increases steadily in a small scale, and there is no spring-back displacement of shaft.

By comparison, scenario II is better in controlling the shaft deformation than scenario I, and the maximum shaft displacement is 9.7 mm when the XI# ore body is excavated completely. Although the maximum displacement does not exceed the safety threshold 10 mm, the MPI value at step 5 is too low, which means that the ore production within the distance of 100 m from the shaft is small but the influence on the shaft displacement is significant; as a result, this part of ore is suggested to be left as the shaft pillar. Compared to the original shaft pillar delineated according to the rock movement angles, more than 1000 kt ore can be mined out.

Table 9: Details of scenario II.

Simulative excavating steps	Mineral output/kt	Ore proportion/%	Shaft displacement/m	Displacement proportion/%	MPI
1	264.19	15.62%	0.0012	12.71%	1.23
2	363.85	21.51%	0.002	20.88%	1.03
3	563.42	33.30%	0.0026	26.26%	1.27
4	395.06	23.35%	0.0025	25.36%	0.92
5	105.20	6.22%	0.0014	14.79%	0.42
In total	1691.71	100.00%	0.0097	100%	1.00

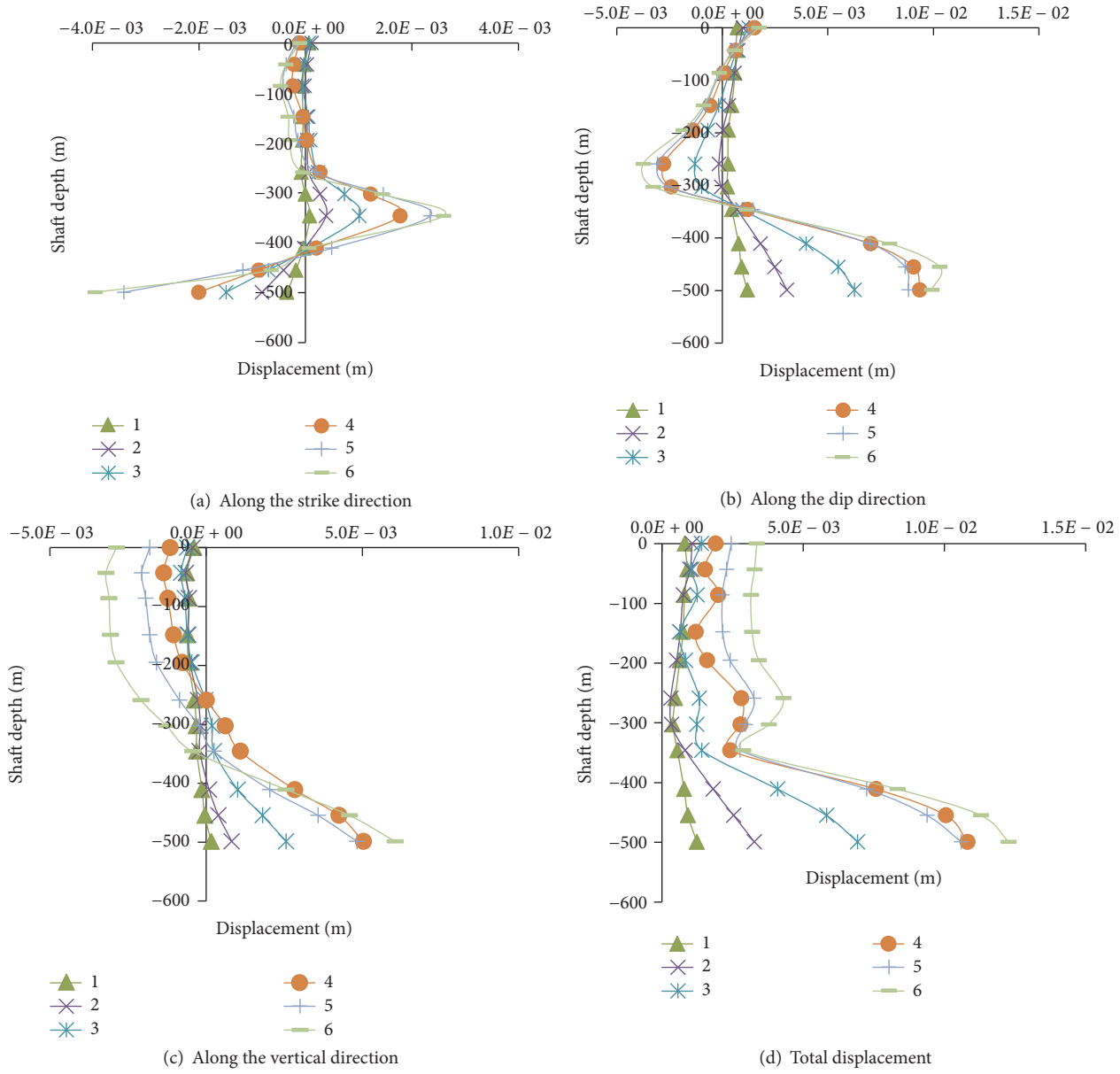

Figure 16: Shaft displacement during mining with scenario I.

According to the numerical simulation, the max shaft displacement at −380 m level is 1.6 mm at this time, and the monitoring shaft lateral displacement is 1.4 mm. In this regard, we deem that the numerical simulation results are well in agreement with the monitoring data; of course, it needs to be validated further against the in situ monitoring for a long time. Even so, the main value of this crude numerical model mainly comes from the comparison with itself; by this way, a better mining sequence and a proper mining boundary are obtained.

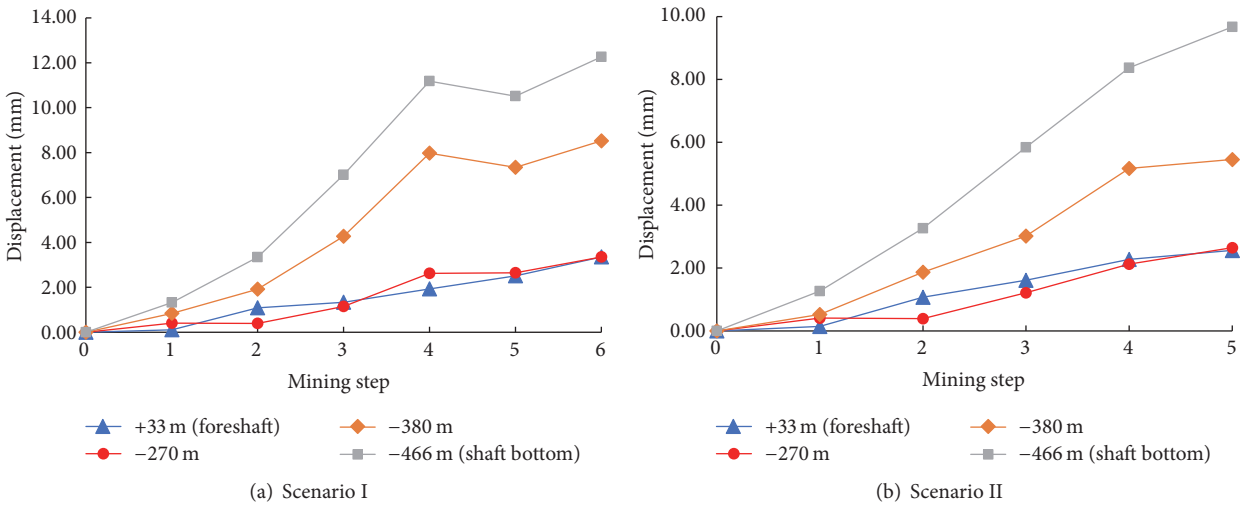

(a) Scenario I (b) Scenario II

Figure 17: Shaft displacement at 4 positions during mining with scenarios I and II.

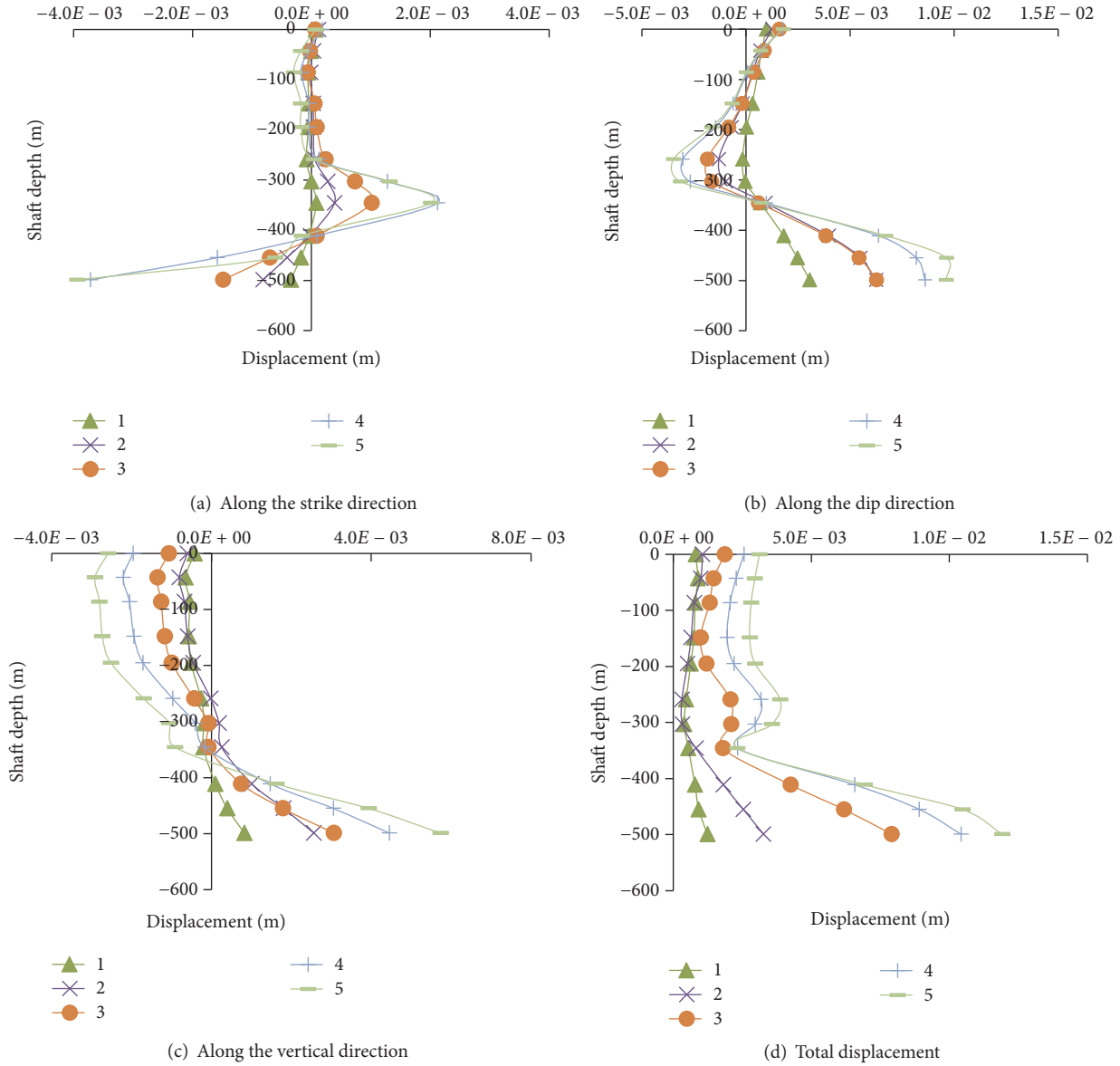

(a) Along the strike direction (b) Along the dip direction

(c) Along the vertical direction (d) Total displacement

Figure 18: Shaft displacement during mining with scenario II.

7. Discussions and Conclusions

In this paper, the effects of mining activates on the stability of the main mine shaft at the Xincheng Gold Mine in China were investigated by means of in situ monitoring and numerical simulation; the following conclusions are drawn:

(1) By means of orthogonal design experiment and numerical simulation, sensitivities of the five main factors affecting the shaft displacement have been studied. Dip of the ore body, lateral pressure coefficient, and distance between the shaft and mined-out area are significant factors affecting the shaft displacement.

(2) The Mining Priority Index (MPI) has been defined in order to quantify the relationship between the mineral output and shaft displacement, and then, the optimal mining sequence is selected according to the ranking of MPI values. The MPI is simple but practical, which can be of reference to other similar mining projects.

(3) Based on in situ displacement monitoring and numerical simulation, we deem that the numerical simulation results are generally in agreement with the monitored ones. Thus the numerical simulation is validated against the in situ monitoring up to now. It indicates that excavation of the XI# orebody is tolerable if the ore within a distance of 100 m away from the shaft is kept as pillars, and the original shaft pillar delineated according to the rock movement angles is too conservative.

With the advancing of mining activities, both the in situ monitoring and numerical simulation should be conducted to trace and predict the mining-induced responses of shaft. Of course, the numerical model established at present is relatively rough; a more sophisticated numerical model with detailed stope design should be established in the future. Based on that, a more detailed mining sequence also can be optimized by means of ranking the MPI values.

Conflicts of Interest

The authors declare that they have no conflicts of interest.

Acknowledgments

The support provided by the National Key Research and Development Program of China (Grant no. 2016YFC0801607), the National Natural Science Foundation of China (Grant nos. 51525402, 51404067, 51374049, and 51534003), and Fundamental Research Funds for the Central Universities of China (Grant nos. N160104005 and N160103005) is gratefully acknowledged. Moreover, this work was accomplished with the assistance of Xincheng Gold Mine; the authors would like to acknowledge the contributions of mine personnel at Xincheng Gold Mine.

References

[1] S. Budavari and R. W. Croeser, "Effects of the extraction of tabular deposits around vertical shafts in deep-level mines.," *Proc. 6th congress International Society for Rock Mechanics, Montreal, 1987. Vol. 2*, pp. 825–828, 1987.

[2] S. D. McKinnon, "Alternatives to shaft pillars for the protection of deep vertical shaft systems," in *Proceeding of the 6th International Conference on Rock Mechanics*, vol. 2, pp. 1129–1134, Montreal, Canada, 1987.

[3] J. W. Klokow and S. L. Mulder, "Early shaft reef removal at Beatrix No 3 Vertical Shaft," in *Proceeding of the 10th ISRM Congress*, pp. 249–254, Sandton, South Africa, 2003.

[4] Y. Fujii, D. Ishijima, and M. Igarashi, "Shaft damages due to mining," in *Proceedings of the 7th ISRM Congress*, pp. 16–20, Aachen, Germany, 1991.

[5] J. C. Johnson and S. A. Orr, "Rock mechanics applied to shaft pillar mining," *International Journal of Mining and Geological Engineering* , vol. 8, no. 4, pp. 385–392, 1990.

[6] G. D. T. Judeel, "Study of the effects of shaft pillar extraction on a vertical shaft located in highly stratified and poor quality rock masses," in *Proceeding of the 10th ISRM Congress*, Sandton, South Africa, 2003.

[7] J. McMullan, W. F. Bawden, and R. Mercer, "Excavation of a shaft destress slot at the Newmont Canada Golden Giant Mine," in *Proceedings of the Proceeding of the 6th North America Rock Mechanics Symposium (NARMS)*, p. 5, 2004.

[8] G. Bruneau, D. B. Tyler, J. Hadjigeorgiou, and Y. Potvin, "Influence of faulting on a mine shaft-a case study: Part I-Background and instrumentation," *International Journal of Rock Mechanics and Mining Sciences*, vol. 40, no. 1, pp. 95–111, 2003.

[9] G. Bruneau, M. R. Hudyma, J. Hadjigeorgiou, and Y. Potvin, "Influence of faulting on a mine shaft-a case study:Part II-Numerical modelling," *International Journal of Rock Mechanics and Mining Sciences*, vol. 40, no. 1, pp. 113–125, 2003.

[10] Q.-L. Zhao, Q. Gao, Z.-P. Zhang, and W.-G. Xiao, "Deformation Analysis and Stability Evaluation of the Main Shaft at Jinchuan Mine," *Journal of China University of Mining and Technology*, vol. 17, no. 2, pp. 290–294, 2007.

[11] M. M. Khan and G. J. Krige, "Evaluation of the structural integrity of aging mine shafts," *Engineering Structures*, vol. 24, no. 7, pp. 901–907, 2002.

[12] P. Huang, C. Chen, and G. Xiao, "Feasibility analysis on using shaft in the region with large deformation," in *Proceedings of the 1st International Symposium on Mine Safety Science and Engineering, ISMSSE 2011*, pp. 1726–1730, China, October 2011.

[13] H. Kratzsch, *Mining Subsidence Engineering*, Springer Berlin Heidelberg, Berlin, Heidelberg, 1983.

[14] M. F. Cai, L. Qiao, and C. H. Li, "Measuring results and regularity of in situ stress in Xincheng gold mine," *Nonferrous Metals*, vol. 52, no. 3, pp. 1–6, 2000 (Chinese).

[15] *The State Bureau of Safe Production Supervision and Administration, GBl6423-2006 Safety Regulations for Metal and Nonmetal Mines*, vol. 62, GBl6423-2006 Safety Regulations for Metal and Nonmetal Mines, 2005.

[16] E. Hoke, C. Carranza-Torres, and B. Corkum, "Hoek-Brown failure criterion," in *Proceedings of NARMS-TAC2002, Mining Innovation and Technology*, Toronto, 2002, 2672ng I.

[17] E. Hoek and E. T. Brown, "Practical estimates of rock mass strength," *International Journal of Rock Mechanics and Mining Sciences*, vol. 34, no. 8, pp. 1165–1186, 1997.

[18] S. Shnorhokian, H. S. Mitri, and D. Thibodeau, "Numerical simulation of pre-mining stress field in a heterogeneous rockmass," *International Journal of Rock Mechanics and Mining Sciences*, vol. 66, pp. 13–18, 2014.